

Analysis of directional wave fields using X-band navigation radar

J.C. Nieto Borge ^{a,*}, C. Guedes Soares ^b

^a *Puertos del Estado, Clima Marítimo, Antonio López, 81, 28026 Madrid, Spain*

^b *Unit of Marine Technology and Engineering, Technical University of Lisbon, Instituto Superior Técnico Av. Rovisco Pais, 1049-001 Lisbon, Portugal*

Abstract

The aim of this work is to present an approach to describe complex sea states including the ones consisting of superpositions of swell and wind sea components, using a nautical radar in X-band as a remote sensing technique. In the present article, the inversion method to obtain the spectral representation of the wave fields is described. The method is applied to analyse data obtained from simulation techniques, as well as from measurements obtained during oceanographic campaigns in the Bay of Biscay and North Sea. © 2000 Elsevier Science B.V. All rights reserved.

Keywords: Sea state; Directional spectrum; Waves; Currents; Nautical radars

1. Introduction

Much of the wave data necessary for long term and extreme predictions that are the support for design and operational decisions regarding coastal and offshore structures has been collected by waverider buoys. This requires that extensive measuring programs be conducted in a specific location before a long-enough database has been collected.

To overcome this problem it is necessary to use all available data that can characterise a given area and combine it. This objective has been pursued in the WAVEMOD project, which has compared the accuracy and consistency of different types of data,

* Corresponding author.

E-mail addresses: joscar@puertos.es (J.C. Nieto Borge), guedess@alfa.ist.utl.pt (C. Guedes Soares).

using as common reference the waverider buoy (Guedes Soares, 1995). This paper deals with one additional type of data, in which wave height estimations obtained from an X-band navigation radar installed in a coastal station are compared with the ones of a directional waverider buoy.

The use of the navigation radar for estimating the directional wave spectra is relatively recent since some of the earlier references are Oudshoorn (1960) and Mattie and Harris (1979). The radar has some clear advantages in coastal monitoring in that it obtains spatial information in a range of about few kilometers, depending on the characteristics of the site in which it is installed. It is not liable to accidents such as the drifting of buoys as a result of being hit by fishing equipment for example.

Because the radar is in a fixed position, it takes successive images of the same location, which allows a spectral estimate without the directional ambiguity associated with the SAR images (Young et al., 1985).

This paper presents the theoretical background to the estimation of the directional spectra and the prevailing current. It provides the comparisons with the directional spectra estimated from buoy data, showing good accuracy and consistency of the results. It is even shown that the radar has a better directional discrimination than a directional buoy, which is especially important for bimodal sea states.

2. Theoretical background

2.1. Stochastic description of sea states

Sea states correspond to wave fields with invariant statistical properties along the position \vec{r} and the time t . So, the wave fields with these features are homogeneous in the spatial dependence and stationary in the time evolution. The free surface elevation of a sea state $\eta(\vec{r}, t)$ has the following spectral representation

$$\eta(\vec{r}, t) = \sum_{\Omega_{\vec{k}, \omega}} e^{i(\vec{k} \cdot \vec{r} - \omega t)} dZ(\vec{k}, \omega), \quad (1)$$

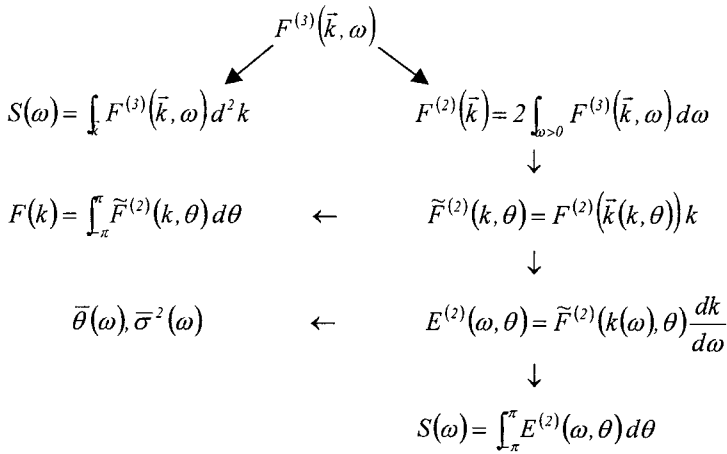
where \vec{k} , is the wave number and ω is the angular frequency, $\Omega_{\vec{k}, \omega} \equiv [-\vec{k}_c, \vec{k}_c) \times [-\omega_c, \omega_c)$ is the admissible domain of the spectral variables, being \vec{k}_c and ω_c , the Nyquist limits for the wave number and frequency, respectively. $dZ(\vec{k}, \omega)$ is the spectral random measure, which is usually considered as a gaussian random variable. They are statistically uncorrelated for different wave components (\vec{k}, ω) .

Under these conditions η is a linear, homogeneous and stationary zero-mean stochastic process, described by a three-dimensional power spectrum defined as

$$F^{(3)}(\vec{k}, \omega) d^2 k d \omega = E \left[dZ(\vec{k}, \omega) dZ^*(\vec{k}, \omega) \right], \quad (2)$$

E being the expectation operator and the upper index $*$ means the complex conjugate.

Table 1
Spectral representations of a sea state



There is a dependency between \vec{k} and ω for linear waves given by the dispersion relationship

$$\omega = \varpi(\vec{k}) = \sqrt{gk \tanh(kd)} + \vec{k} \cdot \vec{U}, \tag{3}$$

where d is the water depth $k = \|\vec{k}\|$ and $\vec{U} = (U_x, U_y)$ is the current velocity, which induces a Doppler shift.

Taking into account Eq. (3), it is possible to obtain different spectral densities depending on other variables (see Table 1), such as the frequency $f = \omega/2\pi$ or the wave propagation direction θ . The integral of all of these spectral densities, over their specific domain, must keep the value of the total variance of the stochastic process. So, the ordinary directional spectrum in frequency and direction $E^{(2)}(\omega, \theta)$ can be estimated, as well as other common spectral representation of wave properties, such as frequency spectrum $S_f(\omega)$, main direction $\bar{\theta}(\omega)$, angular spreading $\bar{\sigma}^2(\omega)$, cross-spectra $(C_{mnf}(\omega), Q_{mnf}(\omega))$, etc.

2.2. Navigation radar images from wave fields

The measurement of sea states using nautical radars is based on the backscatter of the electromagnetic fields by the ripples and the roughness of the free sea surface due to the local wind. So, to obtain wave information from radar images, the presence of wind blowing over the sea is necessary. This pattern of returned electromagnetic energy is modulated by the larger structures, such as swell and wind sea waves, which are the aim of the method. The final pattern shown on the radar screen is known as *sea clutter*. Fig. 1 shows an example of a sea clutter taken from a radar station on shore located at the

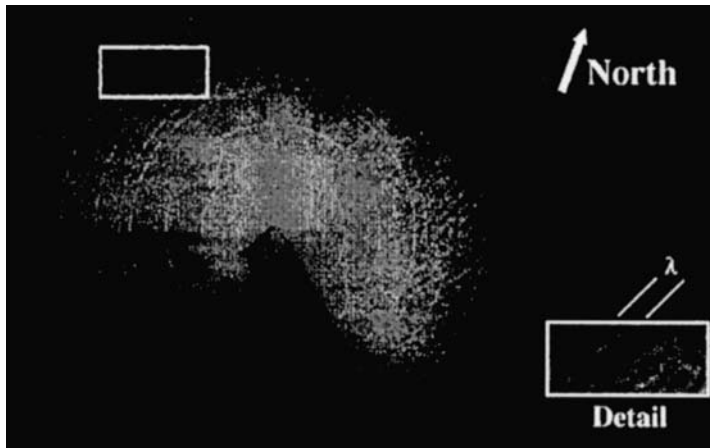


Fig. 1. Example of sea clutter.

Northern coast of Spain (Bay of Biscay), where the wave refraction due to the variable bathymetry can be observed (Nieto, 1997).

Unlike other remote sensing systems, such as SAR on board satellites, navigation radar images cover small areas. However, these sensors are able to obtain temporal information about sea states using consecutive rotations of the antenna. Hence, it is possible, to know the spatial and the time evolution of wave fields.

In the radar imaging mechanism different phenomena are present, which are responsible for the final image shown on the radar screen. The main aspects are the following.

- Range dependence. Radar image intensity is lower for larger distances due to the decay law of the received electromagnetic energy with the distance. This effect introduces a static pattern in the radar image spectrum.

- Azimuthal dependence. The intensity of the image depends on the wind direction. So, the return is higher in the direction where the wind is coming from.

- Wind speed dependence. The image intensity increases as the wind grows.

- Tilt modulation. This is related to the effective slope of the waves. So, the facets with an orientation close to the antenna direction produce higher backscatter than the others. The tilt modulation increases the spectral energy for high wave numbers.

- Shadowing modulation. Shadowing is a non-linear phenomena that introduces additional components of \vec{k} and ω in the radar image spectrum. This effect occurs when the higher waves hide the lower waves to the radar antenna illumination, and is especially important in marine radar imaging due to the grazing incidence (Nieto, 1997; Seemann, 1997).

- Hydrodynamic and orbital modulation. They are due to the motion of the water and its particles, producing grouping in the ripple structure, which induces changes in the returned energy.

In analysing radar image spectra, it can be realised that all of these phenomena produce distortions in the wave spectrum (Ziemer and Rosenthal, 1987). The main effects are static patterns for very low frequencies and more energy for high wave

numbers and frequencies. So, to obtain a good estimation of the wave spectra, it is necessary to understand properly how the spectral energy is distributed in the three-dimensional image spectrum.

3. Wave spectrum estimation from radar images

The first procedure to analyse wave fields with a nautical radar is to obtain time series of N_t , consecutive rectangular subareas of sea clutter images (Fig. 2). In this case, the sampling time is the antenna rotation period. All the data set in this work was obtained using the Wave Monitoring System (WaMoS). This device samples the analogue video signal from the radar unit in a set of digital grey levels to be analysed by a computer (Dittmer, 1995).

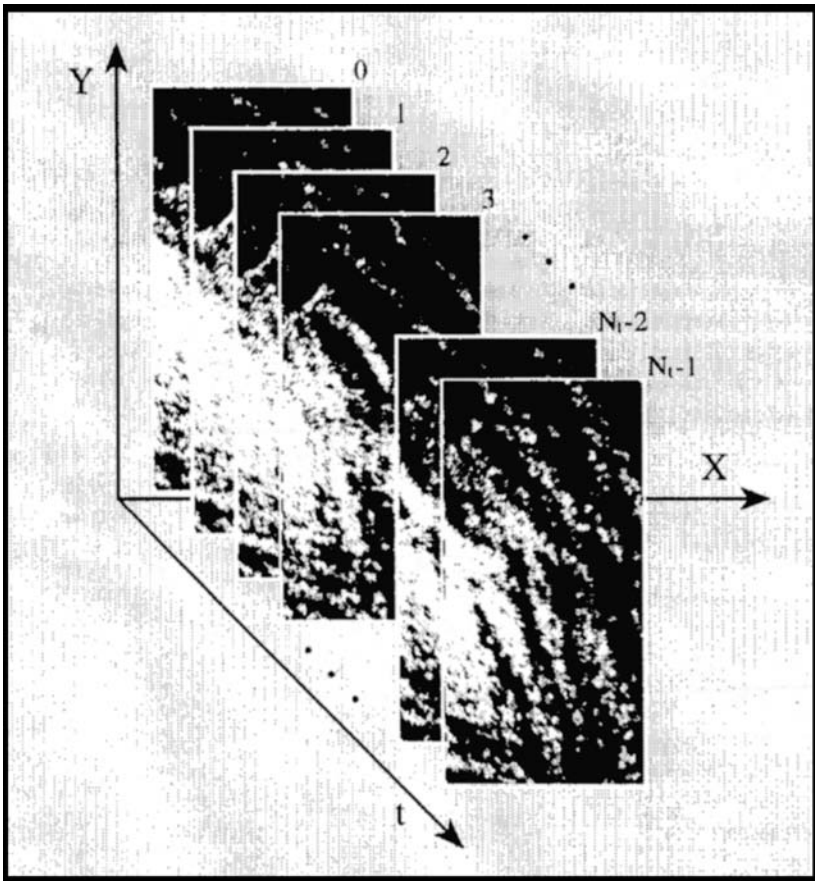


Fig. 2. Radar subimage time series sailed with WoMoS A/D converter.

There is a variability in the spectral estimation for the azimuth situation of the subimages. This effect is mainly due to the azimuthal dependence of the backscatter with the wind direction (Reichert, 1994) and the tilt modulation that produces a distortion of wave fronts for positions close to the antenna. So, for practical purposes, it is better to use the rectangular subareas (or subimages) with a wider longitude in azimuth. In this way, an average is produced for the different orientations of the antenna inside the same subimage.

The subimage time series is considered as a stochastic process depending on the space and time $\psi(\vec{r}, t)$.

Using a three-dimensional discrete Fourier transform (DFT) algorithm the estimation of the image spectrum $F_{\psi}^{(3)}(\vec{k}, \omega)$ is obtained. In order to get good estimators of the corresponding wave spectrum and the related sea state parameters, it is necessary to apply an inversion modeling technique. The steps to reach this goal are described below (Nieto, 1997).

3.1. Image normalisation

This technique is performed by subtracting the mean intensity of the sea clutter image time series to avoid the main contribution of the static patterns in space and time present in the data set.

3.2. Spectral estimation

Application of a three-dimensional FFT algorithm to obtain the estimation of the image spectrum or image periodogram $F_{\psi}^{(3)}(\vec{k}, \omega)$.

3.3. Applying low-pass filter to $F_{\psi}^{(3)}(\vec{k}, \omega)$ to remove the static pattern

The purpose of this step is to eliminate the non-stationary and non-homogeneous trends in the subimage time series. A good empirical threshold for frequency of the high-pass filter is $\omega_{th} = 2\pi \cdot 0.03$ rad/s (lower frequencies may not be considered as swell or wind sea cases). The filter is defined as:

$$F(\vec{k}, \omega) = \begin{cases} 0; & \text{if } (\vec{k}, \omega) \in \Omega_F, \\ 1; & \text{otherwise} \end{cases} \quad (4)$$

where Ω_F is the set in the three-dimensional spectral domain defined by the very low wave numbers and frequencies that do not belong to the wave field.

$$\Omega_F \equiv \left\{ \vec{k} \in [-\vec{k}_c, \vec{k}_c] : \|\vec{k}\| \leq k(\omega_{th}) \right\} \times [-\omega_{th}, \omega_{th}], \quad (5)$$

$k(\omega_{th})$ being the wave number solution of the dispersion relationship without current. In this case, k is very small. Hence, the dot product $\vec{k} \cdot \vec{U}$ is small as well, and it can be eliminated from the dispersion relationship formula.

The filter (Eq. 4) could be considered too sharp in the spectral domain (\vec{k}, ω) . In this case, it is possible to use a transition volume inside the domain Ω_F , where the filter

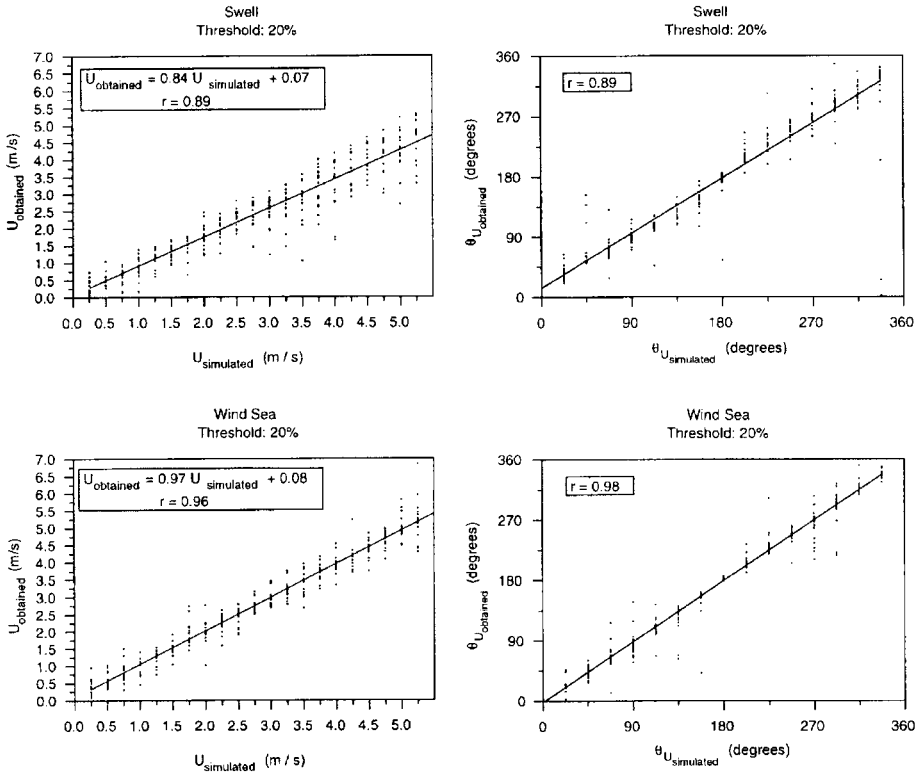


Fig. 3. Estimation of the Doppler shift current (norm and relative going-to direction to the wave field) for simulated sea states of swell and wind sea.

takes values from 0 to 1 smoothly, by applying a cosine square function for example. In general, this is not necessary because the wave energy is far enough, in the $\Omega_{\vec{k}, \omega}$ domain, from the static pattern. So, a simple filter, as indicated in Eq. (4), is enough to analyse the wave energy distribution in the image spectrum.

3.4. Estimation of the doppler shift due to the current

Once, the non-homogeneous and non stationary spectral energy has been eliminated from the function $F_{\psi}^{(3)}(\vec{k}, \omega)$, the next step is to match the information of the \vec{k} and ω spaces, analysing the distribution of this energy in the Nyquist domain $\Omega_{\vec{k}, \omega}$. The physical model, which has to be applied, is the linear wave theory, which means the dispersion relationship (Eq. 3). So, assuming that the wave energy is a first order contribution to the total image spectral energy, which can be proved using simulated radar images, as well as real measurements, the current \vec{U} can be estimated by minimising the next functional:

$$v = \sum_{j=1}^{N_r} \left[\omega_j - \varpi(k_{x_j}, k_{y_j}) - k_{x_j} U_x - k_{y_j} U_y \right]^2, \tag{6}$$

where $\overline{\omega}_0(k)$ is the dispersion relationship formula without current and N_r is a number of (\vec{k}, ω) points whose spectral energy is due to the wave field and not due to other effects in the radar imaging.

Using numerical simulation methods of sea states and their associated radar images, N_r is estimated from all points with energy higher than 20% of the maximum value of $F_{\psi}^{(3)}(\vec{k}, \omega)$ (Nieto, 1997). Fig. 3 shows the results for the threshold of 20% of the spectral peak. These simulations have been carried out using a Wallops spectrum (Huang et al., 1983) for swell and JONSWAP spectrum (Hasselmann et al., 1973) for wind sea. The simulated directional spreading function follows the Mitsuyasu parameterisation

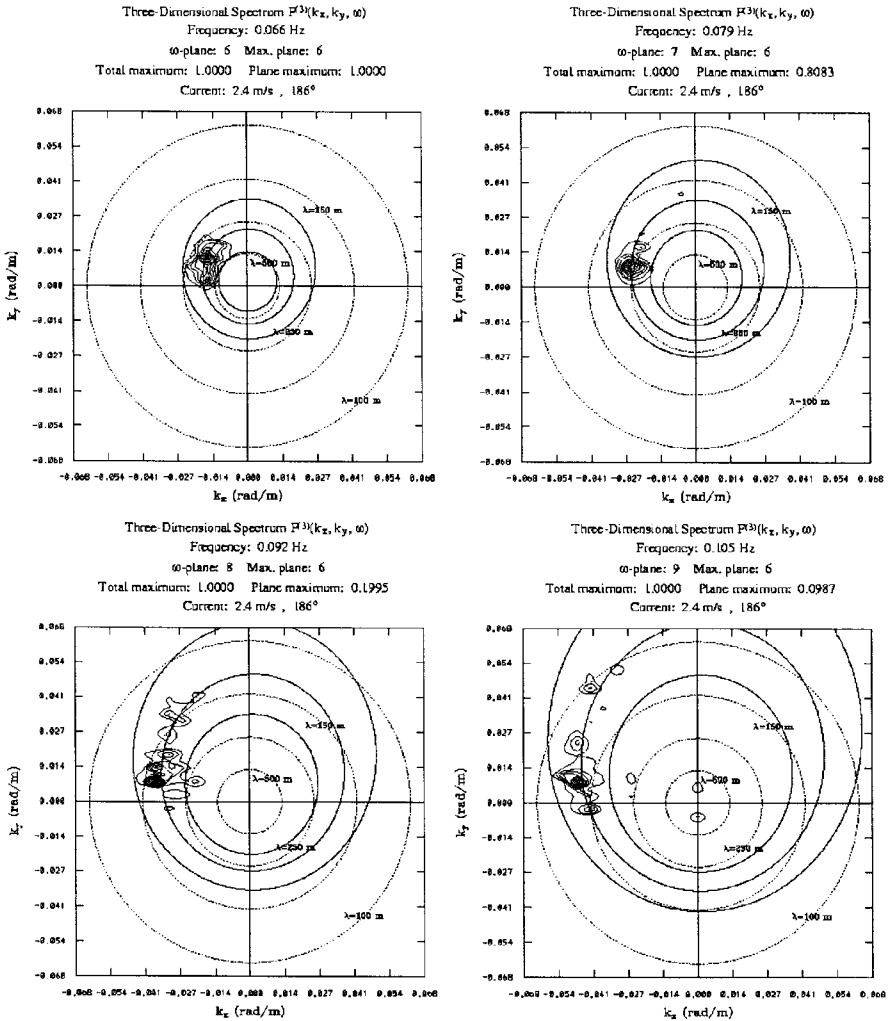


Fig. 4. Spectral energy for different frequency planes and current estimation.

(Mitsuyasu, 1975). The stochasticity of the simulated wave fields is imposed by applying uniformly distributed random phases and the spectral variability as a χ^2 probability distribution function. To simulate the radar imaging a geometric optics approximation is used for the shadowing and the projection of the normal exterior vector to the sea surface over the antenna illumination direction for the simulation of the tilt modulation (Nieto and Alfonso, 1994).

Fig. 4 shows four frequency planes of the high-pass filtered image spectrum obtained from a measurement taken in Cantabrian Sea with a ship moving at 5 knots during the experiment EXBAYA-1995 (February, 1995). This is a swell case, which is the typical wave situation in the Bay of Biscay.

In these figures, a confidence band in \vec{k} space has been built, taking into account the dispersion relationship curves for the lower and upper frequencies for each frequency plane. The reason for this is that for a DFT there is a resolution in the spectral energy of each frequency given by twice the sampling frequency $\Delta\omega$. So, the energy of the frequency ω_v ($v = 0, \dots, N_t/2$) is the total contribution of the energy for frequencies bigger than ω_{v-1} and smaller than ω_{v+1} . The spectral energy due to the wave field is distributed around this confidence band.

The fitted current $\vec{U} = (U_x, U_y)$ is the total contribution of several effects, such as relative motion between the observer and the wave field, currents induced by tides, by the wind, by the waves and other currents associated to the oceanic circulation.

3.5. Filtering the spectral energy outside the dispersion relationship

When the components of the current (U_x, U_y) have been fitted, the next step is to remove all energy not due to the wave field. For this purpose, the dispersion relationship (Eq. 3) is used (Young et al., 1985).

Taking into account the DFT theory and the dispersion relationship $\omega(\vec{k})$, there is an error in \vec{k} for each frequency plane ω_v .

$$\delta k_v = \|\vec{k}(\omega_{v+1})\| - \|\vec{k}(\omega_{v-1})\|; \quad v = 0, \dots, N_t/2. \tag{7}$$

The image spectrum can be filtered (Young et al., 1985), obtaining an estimation of the wave spectrum

$$F_f^{(3)}(\vec{k}_{mn}, \omega_v) = \begin{cases} F_\psi^{(3)}(\vec{k}_{mn}, \omega_v); & \text{if } \|\vec{k}_{mn} - \vec{k}(\omega_v)\| \leq \delta k_v, \\ 0; & \text{otherwise} \end{cases} \tag{8}$$

where \vec{k}_{mn} represents the sampling of the wave number discretization by the three-dimensional DFT output.

Because the function $\omega = \omega(\vec{k})$ is not linear, the size of this filter in the \vec{k} space depends on ω_v . It is possible to make the filter have the same size in the \vec{k} space, adding a new quantity $\Delta k(\omega_v)$. That is

$$\delta k_v \mapsto \delta k_v + \Delta k(\omega_v). \tag{9}$$

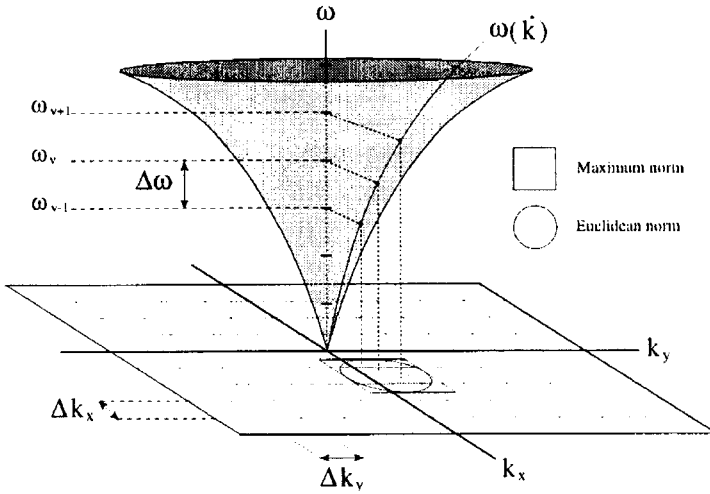


Fig. 5. Scheme of the filter in (\vec{k}, ω) space.

The $\Delta k(\omega_v)$ values must be smaller or of the same order than the sampling wave numbers Δk_x and Δk_y . For practical purposes, $\Delta k(\omega_v)$ can be set to 0.

Fig. 5 shows a scheme about how the filter (Eq. 8) works in the \vec{k} space using the dispersion relationship shell. For currents of high intensity, the dispersion relationship has two available solutions of \vec{k} when $\vec{k} \cdot \vec{U} < 0$ (Fig. 6). In these zones there are no solutions for frequencies larger than a value ω_M . This frequency has a double solution of the wave numbers with the same value. The algorithm used to solve the wave number value must be robust for these cases.

Once the three-dimensional spectrum has been filtered, it is possible to integrate the function $F_f^{(3)}(\vec{k}, \omega)$ over all the positive frequencies to obtain a two-dimensional spectrum depending only on the wave vector $F_f^{(2)}(\vec{k})$ as well as other spectral descriptions of sea states as Table 1 shows.

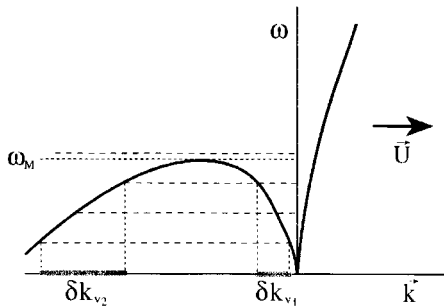


Fig. 6. Dispersion relationship solutions for $\vec{k} \cdot \vec{U} < 0$.

4. Comparison of the radar results with a directional buoy

Some of the data shown in this section were taken from the EXBAYA 95 oceanographic campaign in February of 1995, (Nieto, 1997) measuring with a ship-borne nautical radar in the vicinity of a pitch-roll directional buoy moored in deep waters (600-m depth).

4.1. Description of the data sets

During the experiment, several cases of swell coming from Northwest were measured. This is the typical sea state situation in the Bay of Biscay. These incoming wave fields are generated by storms in Northern Atlantic Ocean arriving to the North of the Iberian Peninsula as very long grouped waves.

The system used was a conventional nautical X-band radar working in short pulse in order to get the maximum available spatial resolution. The radar measurement is composed by time series of 32 consecutive sea clutter images spatially sampled in 128×256 pixels. The spatial resolution is given by the range and azimuthal resolution of the radar antenna. In this case, each pixel has an area of $9.6 \times 9.6 \text{ m}^2$. The sampling time in the time series is given by the antenna rotation period, which was 2.6 s for this receiver.

The used buoy is a conventional moored directional pitch-roll buoy, which provides three time series (heave, wave slope along West–East and wave slope along South–North). The sampling time is 1 s, 2048 s being the total duration of each measurement.

The directional spectra $E^{(2)}(f, \theta)$ were estimated from these data using the following three methods

- Extended Maximum Likelihood Method (EMLM) (Isobe et al., 1984)
- Maximum Entropy Method (AR(2)) (Lygre and Krogstad, 1986)
- Gaussian Instantaneous Direction Method (GIDM) (Egozcue and Arrivas, 1991).

4.2. Results

4.2.1. Directional spectrum

Some example of interpolation for the $E^{(2)}(f, \theta)$ spectrum from the buoy records and the corresponding estimation from the sea clutter time series can be seen in Fig. 7. This measurement corresponds to a swell wave field coming from North–north-west approximately.

The interpolation methods from buoy records have some limitations in the estimation of $E^{(2)}(f, \theta)$ because the buoy can only measure few properties of the wave field in a fixed point of the ocean. In this case, the number of wave properties are three, the heave and the two slopes. It is well known that the correct estimation of $E^{(2)}(f, \theta)$ is impossible when measuring only a limited number of sea state features. This is a big problem in cases of multimodal sea states (i.e. superposition of one or two swells and a wind sea) (Nieto and Alfonso, 1993).

Each estimation of $E^{(2)}(f, \theta)$ obtained from buoy records can provide quite different results depending on the behaviour of the analysed sea state but keeping the spectral properties of measured time series. EMLM (Fig. 7a) provides more background directional noise than the other estimations (AR(2) and GIDM). AR(2) (Fig. 7b) presents some problems in the estimation of the directional spectrum from a very focused sea state, such as a very long swell (Nieto and Alfonso, 1993). This behaviour is due to the intrinsic bimodality of this method. GIDM (Fig. 7c) provides a directional average in case of symmetrical bimodal sea states. Further comparisons among methods of estimation of the directional spectrum can be found in (Guedes Soares and Cavaco, 1997).

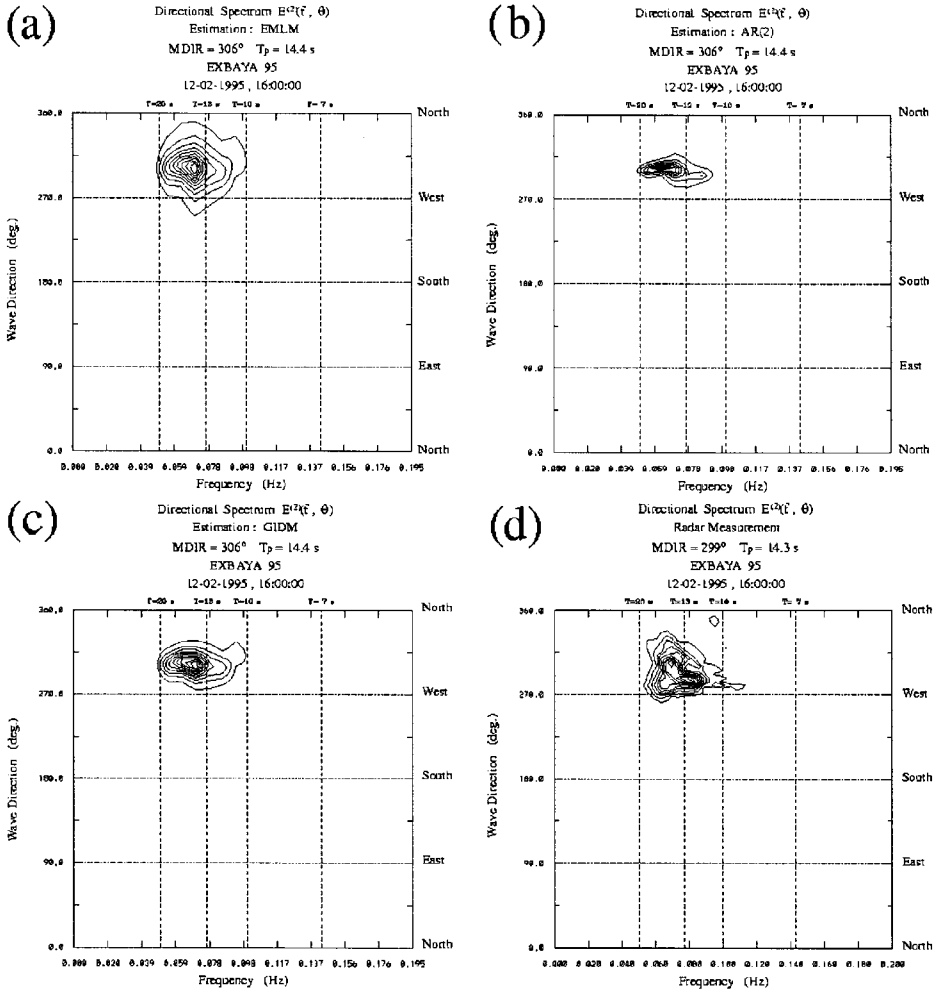


Fig. 7. Estimation of $E^{(2)}(f, \theta)$ from EMLM (a), AR(2) (b), GIDM (c) and radar (d).

The estimation from the radar sea clutter appears in Fig. 7d. The nautical radar has more directional resolution than a buoy because this system provides spatial information about the wave fields. An example of bimodal sea state can be seen in Fig. 8. This measurement was taken in the North Sea during the ERS-1/ERS-2 Tandem campaign.

The radar measurement is only possible when a local wind field is present. The necessary minimum wind velocity to obtain electromagnetic energy return from the sea surface depends on each installation and the values of the emission power, the antenna

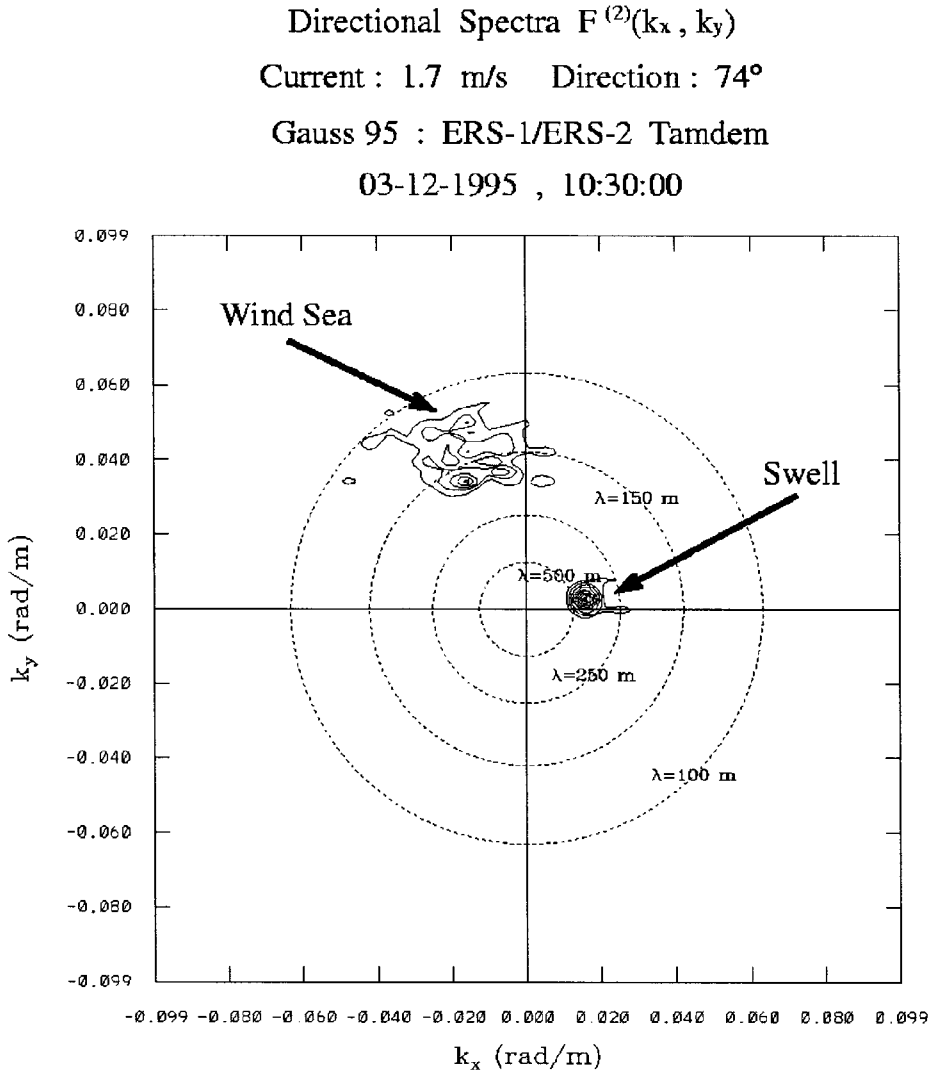


Fig. 8. Bimodal wave number spectrum.

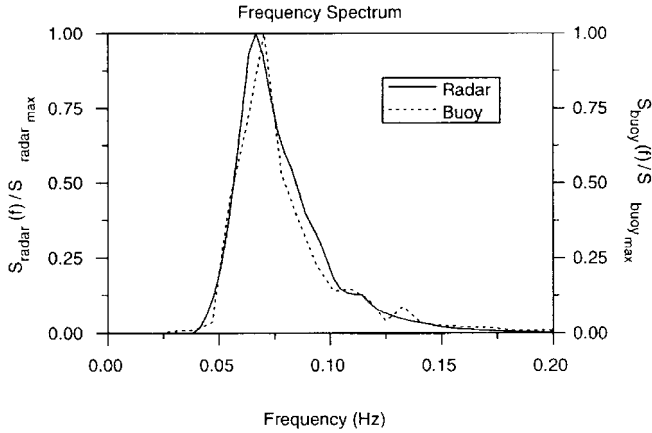


Fig. 9. Frequency spectrum.

gain and the angle of incidence. For a ship-borne conventional system, the threshold value for the wind is around 3 m/s.

4.2.2. Frequency spectra

Once the $E^{(2)}(f, \theta)$ is obtained, the one-dimensional spectrum as well as other parameters depending on the frequency can be computed. As mentioned above, pitch-roll buoys can only measure three geometric properties of the wave field at a fixed point. So, in order to compare the results from the radar sea clutter analysis with directional buoy data, it is necessary to take into account the limitations of directional buoys in the measurement of the sea state directionality.

Fig. 9 shows one example of frequency spectrum $S(f)$ obtained in the Bay of Biscay at the same location where a pitch-roll buoy was moored. There is a good coincidence in the shape of the two functions. The estimation of coming-from mean direction (MDIR) depending on the frequency $\theta(f)$ from both sensors appears in Fig. 10, as in the case of the one-dimensional spectrum, the comprised $\theta(f)$ from the radar image analysis is

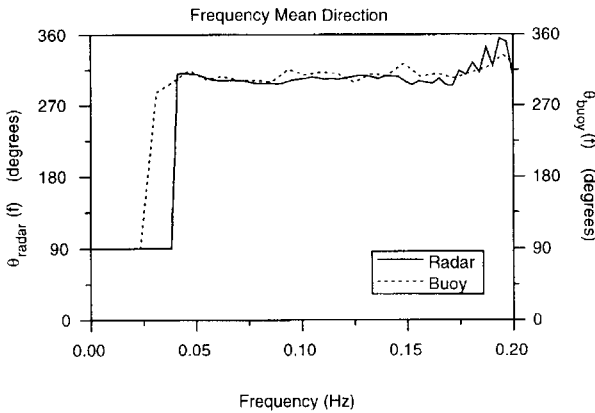


Fig. 10. Mean wave direction (coming-from convention).

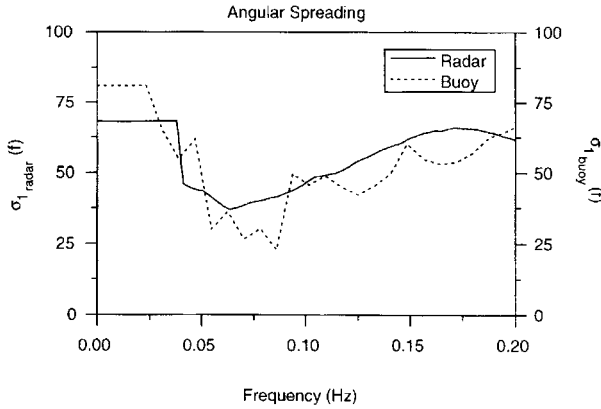


Fig. 11. Angular spreading depending on the frequency.

close to the estimation from the buoy records. The angular spreading can be seen in Fig. 11. The behaviours of the two curves (from buoy and radar respectively) are similar.

Table 2
Comparisons of buoy and radar parameters

Date	Time (GMT)	H _s (m)	MDIR (buoy) (deg)	MDIR (radar) (deg)	T _p (s) (buoy)	T _p (s) (radar)	f _p (Hz) (buoy)	f _p (Hz) (radar)
09-02-95	1155	2.3	301	296	10.8	11.8	0.092	0.085
09-02-95	1158	2.3	301	297	10.8	12.9	0.092	0.078
09-02-95	1200	2.3	301	300	10.8	09.6	0.092	0.104
09-02-95	1203	2.3	301	296	10.8	10.8	0.092	0.092
09-02-95	1206	2.3	301	292	10.8	11.9	0.092	0.084
09-02-95	1500	1.9	306	301	10.4	11.5	0.096	0.086
09-02-95	1502	1.9	306	301	10.4	12.1	0.096	0.082
09-02-95	1505	1.9	306	296	10.4	11.7	0.096	0.085
09-02-95	1508	1.9	306	300	10.4	11.5	0.096	0.086
09-02-95	1511	1.9	306	302	10.4	12.1	0.096	0.082
09-02-95	1514	1.9	306	301	10.4	09.6	0.096	0.104
13-02-95	1200	4.7	302	311	16.5	16.0	0.060	0.062
13-02-95	1202	4.7	302	313	16.5	14.7	0.060	0.068
13-02-95	1205	4.7	302	307	16.5	13.7	0.060	0.072
13-02-95	1208	4.7	302	311	16.5	13.9	0.060	0.071
13-02-95	1211	4.7	302	311	16.5	15.5	0.060	0.064
13-02-95	1214	4.7	302	310	16.5	16.6	0.060	0.060
14-02-95	1500	4.3	305	299	14.4	14.3	0.069	0.069
14-02-95	1502	4.3	305	300	14.4	15.0	0.069	0.066
14-02-95	1505	4.3	305	294	14.4	15.2	0.069	0.065
14-02-95	1508	4.3	305	298	14.4	14.2	0.069	0.070
14-02-95	1511	4.3	305	292	14.4	14.7	0.069	0.068
14-02-95	1514	4.3	305	293	14.4	15.0	0.069	0.067

4.2.3. Integrated wave parameters

Once the one-dimensional spectral functions have been computed the next step is to compare some of the integrated parameters that define a sea state. Table 2 shows the values of the spectral peak frequency f_p , peak period T_p and frequency-integrated MDIR for several measurements taken during the EXBAYA 95 campaign (Nieto, 1997).

Table 2 shows a good agreement between the buoy and the nautical radar for the integrated coming-from MDIR. The spectral peaks for both sensors are in most cases located at the same position. That can be seen in the respective values of f_p or T_p .

5. Conclusions

Nautical radars are a reliable remote sensing technique to measure and monitor directional sea states and surface currents. These sensors provide sea clutter image time series of the spatial and temporal variability of surface wave fields. Those images are analysed and the important sea state parameters can be derived.

One important advantage of nautical radars is in the measurement of multidirectional sea states composed by several single swell and wind sea contributions to the total wave field. In these cases, the radar imaging mechanism provides a more detailed directional description than point measurements. So, the information provided by this system can complement, or in some cases substitute, the data obtained from the analysis of conventional in situ sensors.

Acknowledgements

This work has been carried out in the frame of the WAVEMOD project (MAST-2 contract CT92/0025). The authors want to thank the crew of the vessel Golfo de Vizcaya of the Spanish Maritime Rescue and Safety Institution SASEMAR, where most of the measurements shown in this work were taken from the EXBAYA 95 campaign. In addition, our special thanks to the crew of the German oceanographic vessel Gauss (Bundesamt für Seeschifffahrt und Hydrographie), where some measurements were taken by one of the authors in the ERS-1/2 tandem experiment and to Dr. F. Ziemer for his support and interest in the two oceanographic experiments mentioned above.

References

- Dittmer, J., 1995. Use of Marise Radars for Real Time Wave Field Survey and Speeding up the Transmission/Processing. In: Proc. of the WMO/IOC Workshop on Operational Ocean Monitoring using Surface Based Radars, Geneva, March. pp. 133–137, Report no. 32.
- Egozcue, J.J., Arribas, M.A., 1991. Directional description of ocean waves by the instantaneous direction spreading function. In: Arcilla, A.S., Pastor, M., Zienkiewicz, O.C., Schrefler, B.A. (Eds.), Proc. of Computing Modelling in Ocean Engineering 91 pp. 189–199.
- Guedes Soares, C., 1995. Probabilistic wave modelling in coastal waters. In: Weydert, M., Lipiatou, E., Goni, R., Fragakis, C., Bohle-Carbonell, M., Barthel, K.-G. (Eds.), Marine Science and Technologies vol. 1 Commission of European Communities, pp. 615–628.

- Guedes Soares, C., Cavaco, P., 1997. Analysis of directional spectra from the Portuguese coast. In: Mansard, E. (Ed.), 27th IAHR Seminar on Multidirectional Waves and their Interaction with Structures, San Francisco. pp. 309–322.
- Hasselmann, K., Barnett, T.P., Bouws, E., Carlson, H., Cartwright, D.E., Enke, K., Ewing, J.A., Gienapp, H., Hasselmann, D.E., Kruseman, P., Meerburg, A., Muller, P., Olbers, D.J., Richter, K., Sell, W., Walden, H., 1973. Measurement of Wind–Wave Growth and Swell Decay During the Joint North Sea Wave Project (JONSWAP). Report, German Hydrographic Institute, Hamburg.
- Huang, N. et al., 1983. A study on the spectral models for waves in finite water depth. *J. Geophys. Res.* 88 (C14), 9579–9587.
- Isobe, M., Kondo, K., Horikawa, K., 1984. Extension of MLM for estimating directional wave spectrum. Proc. Symp. on Description and Modelling of Directional Seas, ASCE, paper A-6, 15 pp.
- Lygre, A., Krogstad, H.E., 1986. Maximum entropy estimation of the directional distribution in ocean wave spectra. *J. Phys. Ocean.* 16, 2052–2059.
- Mattie, M.G., Harris, D.L., 1979. A System for Using Radar to Record Wave Direction. Techn. 79-1, US Army Corps of Eng., Coastal Engineering Res. Ctr. Fort, Belvoir., 50 pp.
- Mitsuyasu, H. et al., 1975. Observations of the directional spectrum of ocean waves using a coverleaf buoy. *J. Phys. Ocean.* 5, 750–760.
- Nieto, J.C., 1997. Wave Field Analysis by Using X-Band Nautical Radars. (in Spanish). PhD thesis. Universidad de Alcalá de Henares, Madrid.
- Nieto, J.C., Alfonso, M., 1993. Study of the accuracy and uncertainties of directional wave navigation radar measurements confronted with pitch-roll buoy data. In: Proc. of 12th Int. Conf. On Offshore Mechanics and Arctic Engineering, ASME vol. II pp. 135–142.
- Nieto, J.C., Alfonso, M., 1994. Methods of Sea State Simulation. Publ. No. 56, Puertos del Estado, Dpto. Téc. Clima Marítimo. Madrid.
- Oudshoorn, H.M., 1960. The use of radar in hydrodynamic surveying. In: Proc. of the 7th Conference on Coastal Engineering, Berkeley, California vol. 1 pp. 59–76.
- Reichert, K., 1994. Analysis of the Azimuth Dependence of the Navigation Radar Imaging of the Sea Surface (in German). Diplomarbeit, Fachbereich Geowissenschaften Universität Hamburg.
- Seemann, J., 1997. Interpretation of the structure of the frequency–wave number spectrum of nautical radar temporal sequences of sea states. (in German). PhD thesis. Universität Hamburg, Hamburg.
- Young, I.R., Rosenthal, W., Ziemer, F., 1985. A three dimensional analysis of marine radar images for the determination of ocean waves directionality and surface currents. *J. Geophys. Res.* 90, 1049–1059.
- Ziemer, F., Rosenthal, W., 1987. On the Transfer Function of a Shipborne Radar for Imaging Ocean Waves. Report no 35/96. GKSS-Forschungszentrum Geesthacht, Geesthacht.